Heterotrimeric Kinesin-II Is Required for the Assembly of Motile 9+2 Ciliary Axonemes on Sea Urchin Embryos

Robert L. Morris and Jonathan M. Scholey

Section of Molecular and Cellular Biology, University of California, Davis, California 95616

Abstract. Heterotrimeric kinesin-II is a plus end–directed microtubule (MT) motor protein consisting of distinct heterodimerized motor subunits associated with an accessory subunit. To probe the intracellular transport functions of kinesin-II, we microinjected fertilized sea urchin eggs with an anti–kinesin-II monoclonal antibody, and we observed a dramatic inhibition of ciliogenesis at the blastula stage characterized by the assembly of short, paralyzed, 9+0 ciliary axonemes that lack central pair MTs. Control embryos show no such defect and form swimming blastulae with normal, motile, 9+2 cilia that contain kinesin-II as detected by Western blotting. Injection of anti–kinesin-II into one blastomere of a two-cell embryo leads to the development of chimeric blastulae covered on one side with short, paralyzed cilia, and on the other with normal, beating cilia. We observed a unimodal length distribution of short cilia on anti–kinesin-II–injected embryos corresponding to the first mode of the trimodal distribution of ciliary lengths observed for control embryos. This short mode may represent a default ciliary assembly intermediate. We hypothesize that kinesin-II functions during ciliogenesis to deliver ciliary components that are required for elongation of the assembly intermediate and for formation of stable central pair MTs. Thus, kinesin-II plays a critical role in embryonic development by supporting the maturation of nascent cilia to generate long motile organelles capable of producing the propulsive forces required for swimming and feeding.

INTRACELLULAR transport systems that move and position subcellular cargoes play critical roles in organizing the cytoplasm of eukaryotic cells, by moving and stationing membrane-bounded organelles, driving vesicular transport between these organelles, localizing proteins and RNA molecules, assembling meiotic and mitotic spindles, moving chromosomes, specifying cleavage planes, and contributing to the assembly and stability of flagellar axonemes, for example. Many of these intracellular transport events depend upon the kinesins, a superfamily of microtubule (MT)[1]-based motor proteins that hydrolyze ATP and use the energy released to transport their cargo along MT tracks. Consequently, these motor proteins have a variety of important cellular and developmental functions (Goldstein, 1993; Bloom and Endow, 1994).

The early echinoderm embryo represents an attractive system for studying the functions of MT motor–driven intracellular transport in critical cellular and developmental processes (Wright and Scholey, 1992). For example, MT motor–based transport in these systems is thought to be important for mitosis and cytokinesis (Wright and Scholey, 1992; Wright et al., 1993; Rappaport, 1996), pronuclear migration (Hamaguchi and Hiramoto, 1986), the transport of nuclei before asymmetric cell divisions (Schroeder, 1987), organizing the endomembrane system (Terasaki and Jaffe, 1991), and moving transport vesicles (Pryer et al., 1986; Wadsworth, 1987; Steinhardt et al., 1994; Bi et al., 1997; Scholey, 1996). During early embryogenesis in the sea urchin, MT-based radial transport is likely to deliver new membrane, extracellular matrix material, secretory proteins, and ciliary precursors to the embryonic periphery, culminating in the assembly of cilia at the blastula stage (Auclair and Siegel, 1966; Stephens, 1995), followed by secretion of the "hatching" enzyme that degrades the fertilization envelope, allowing the newly swimming blastula to emerge (Lepage et al., 1992).

Two motor protein complexes, kinesin and kinesin-II, are candidates for driving some of the transport events that occur in cleavage-stage sea urchin embryos. The heterotetrameric kinesin motor protein is thought to transport exocytic vesicles towards the plus ends of astral MTs, delivering these vesicles out to the cell cortex (Scholey et al., 1985; Wright et al., 1991, 1993; Skoufias et al., 1994: Steinhardt et al., 1994; Bi et al., 1997), but the function of

Address all correspondence to Jonathan M. Scholey, Section of Molecular and Cellular Biology, University of California, Davis, CA 95616. Tel.: (916) 752-2271. Fax: (916) 752-1449. e-mail: jmscholey@ucdavis.edu

1. *Abbreviations used in this paper*: MT, microtubule; $SpKAP_{115}$, *Strongylocentrotus purpuratus* kinesin-related protein of molecular mass 85 kD; $SpKRP_{35}$, *Strongylocentrotus purpuratus* kinesin accessory protein of molecular mass 115 kD.

the heterotrimeric motor protein kinesin-II in this system has not yet been reported. Kinesin-II is the first kinesin-related holoenzyme to be purified in its native state from its natural host cell (Cole et al., 1993; Wedaman et al., 1996; Scholey, 1996). It is a heterotrimeric complex containing two heterodimerized motor polypeptides with relative molecular masses of 85 and 95 kD and an associated nonmotor 115-kD polypeptide (Cole et al., 1992, 1993; Rashid et al., 1995; Wedaman et al., 1996). Immunofluorescent localization of kinesin-II reveals a punctate, detergent-sensitive staining pattern of metaphase half spindles and anaphase interzones of sea urchin embryonic cells (Henson et al., 1995) and a punctate, detergent-insensitive staining of the midpiece and flagellar axonemes of sea urchin spermatozoa (Henson et al., 1997). These results, together with data showing that multiple kinesins are present in spindles (Bloom and Endow, 1994) and axonemes (Bernstein and Rosenbaum, 1994), led to the hypothesis that kinesin-II–driven intracellular transport might participate in mitotic spindle and ciliary axoneme assembly and function. To test this hypothesis, we have used antibody microinjection techniques similar to those used previously to investigate the roles of other kinesins in sea urchin embryonic cell division (Wright et al., 1993). We find that the microinjection of a kinesin-II–specific mAb appears to have no effect on mitosis or cytokinesis, but it dramatically inhibits the formation of normal, motile cilia on blastula-stage sea urchin embryos and leads to the production of short, paralyzed cilia that lack central pair MTs. This suggests that kinesin-II–driven intracellular transport plays a critical role in sea urchin embryonic development by delivering ciliary components for ciliogenesis.

Materials and Methods

Materials

The monoclonal antibodies used in these studies were described previously (the antikinesin, SUK-4 in Ingold et al. [1988]; the anti–kinesin-II mAbs in Cole et al. [1993] and Henson et al. [1995]). The control nonspecific mouse IgG antibody was obtained from Sigma Chemical Co. (St. Louis, MO). Wesson canola oil was obtained locally. All other chemicals were obtained from Sigma Chemical Co., or Fisher Scientific (Pittsburgh, PA). *Lytechinus pictus* sea urchins were obtained from Marinus, Inc. (Venice, CA) and kept year round in refrigerated aquaria on an extended daylight cycle, fed with dried kelp (Bodega Farms, Bodega Bay, CA), in sea water collected and filtered at the University of California Davis Bodega Marine Laboratory (Bodega Bay, CA). *Strongylocentrotus purpuratus* sea urchins were collected from tidepools on the northern California coast, north of Bodega Bay, and maintained in 1,000-gallon holding tanks at Bodega Marine Laboratory.

Immunoblotting

High-speed supernatant of *Strongylocentrotus purpuratus* was prepared as described (Buster and Scholey, 1991). MTs were prepared from *S. purpuratus* high-speed supernatant in the presence of AMP-PNP or ATP as previously described (Scholey et al., 1985; Cole et al., 1993; Wedaman et al., 1996). Protein from whole and deciliated *L. pictus* blastulae was prepared by solubilizing pelleted embryos directly in 5× sample buffer (25% glycerol, 0.156 M Tris-HCl, pH 6.8, 5% sodium dodecyl sulfate, 12.5% β-mercaptoethanol, 0.0025% bromophenol blue). *L. pictus* blastulae were deciliated, and the cilia were isolated essentially by the method of Stephens (1986), modified to include an extra centrifugation step to reduce the possibility of cell body contamination of the cilia. Isolated cilia were immediately solubilized in 5× sample buffer. Protein concentrations in sample buffer were determined by the method of Minamide and Bamburg (1990). SDS-PAGE was performed in duplicate on 7.5% resolving gels, and one gel was stained with Coomassie blue while the second gel was transferred to nitrocellulose and probed with K2.4 anti–kinesin-II primary antibody (1.0 or 1.5 μg/ml) overnight at 4°C and then with horseradish peroxidase–conjugated goat anti–mouse secondary antibody (1:2,000) for 1 h at room temperature. Blots were developed using the enhanced chemiluminescence detection system (Amersham Corp., Arlington Heights, IL) exposed for 2 min (*S. purpuratus* MT protein) or 4–20 min (*L. pictus* blastulae protein). For densitometry, 100 μg of blastulae protein, deciliated blastulae protein, and cilia protein were loaded in adjacent lanes and, assuming equivalent protein transfer occurred in adjacent lanes, K2.4-labeled bands were analyzed on Western blots using a Stratagene (La Jolla, CA) Eagle Eye II gel documentation system.

Antibody Preparation, Microinjection, and Image Collection

K2.4 mouse monoclonal antibody for microinjection was prepared from frozen ascites using Affigel protein A and the MAPS II antibody purification system (Bio-Rad Laboratories, Inc., Hercules, CA). SUK-4 was purified essentially as described (Ingold et al., 1988; Wright et al., 1991, 1993). Antibody was then concentrated and exchanged into aspartate injection buffer (AIB: 150 mM potassium aspartate, 100 mM potassium phosphate, pH to 7.2 with potassium hydroxide) using NanoSpin Plus centrifugal devices (10,000 molecular mass cut-off; Gelman Sciences, Ann Arbor, MI). Protein concentration was determined by Bradford microassay with a γ-globulin standard (Bio-Rad Laboratories, Inc.); antibody was diluted to 2.5–10.0 mg/ml in AIB, finally filtered through Ultrafree-MC 0.22-μm filter units (Millipore Corp., Bedford, MA), and stored at 4°C for use within 2 wk. After this period, effects of K2.4 on ciliogenesis began to diminish.

Microinjection of sea urchin embryos was performed by a procedure modified from Kiehart (1982) and Wright et al. (1993). Sea urchin gametes were collected and fertilized according to Wright et al. (1991, 1993). Lateral injection chambers (Kiehart, 1982) allowed high-resolution observation of injections and development and, critical to the success of these experiments, gently restrained the embryos during ciliogenesis at blastula stages. Fertilized eggs were injected with 2.5–5% of cell volume between 20 min after fertilization and the first prometaphase, resulting in an intracellular antibody concentration of ~500 nM. If the injected cell was in early mitosis, antibody was injected at a point distant from the spindle. Embryos routinely survived the injections and reached blastula stage for analysis. Embryos were observed by differential interference contrast microscopy on an inverted microscope (model IM-35; Carl Zeiss, Inc., Thornwood, NY) using a Plan 40× or Planapo 63× objective and imaged as described (Wright et al., 1993). An Argus 10 Image Processor (Hamamatsu Photonics) was occasionally used for contrast enhancement.

Quantitation of Ciliary Properties

To ensure that differences observed between conditions were due to differences in injected agent rather than to variation in batches of eggs, or to exact age of development after fertilization, experimental and control conditions were always performed side-by-side on eggs fertilized at the same time and handled identically. Thus, the quantitative results presented were obtained from embryos under experimental and control conditions lying side-by-side in the injection chamber, although qualitatively identical results were consistently obtained with embryos not included in this paper.

Cell Cycle Length. Embryos were routinely observed to develop at similar rates and reach ciliogenesis within the same 30-min period after 13–14 h of development whether injected or not. To quantitate this observation, values for "Average duration of cell division cycle" (see Table I) were determined for the fourth through seventh cell division cycles for nine embryos from the same batch of eggs, side-by-side in the same injection chamber. Four K2.4-injected embryos, three SUK-4–injected embryos, and two uninjected embryos were observed sequentially, one every 45 s, continuously over a 5-h period. Onset of first observed nuclear envelope breakdown was used as an unambiguous temporal marker for the beginning of the next cell cycle.

Embryonic Motility. K2.4-injected embryos were scored for "Percent blastulae swimming" by two criteria: First, embryos had to develop into morphologically normal round blastulae, and second, nearby control em-

bryos had to be observed swimming (rotating) in the injection chamber at the same time as the K2.4 embryos remained stationary.

Ciliary Motility. To determine "Percent cilia motile" (see Table II) we visually monitored equatorial regions of embryos that were gently compressed between the coverslips of the injection chamber (Kiehart, 1982), where cilia could move freely if they were motile. Equators of such embryos were videotaped, with care being given to capturing images of ciliary bases where each cilium met the surface of its blastomere. After videotaping, the equatorial surfaces of embryos were traced directly from the video monitor onto plastic transparencies, ciliary bases were marked, and each cilium was scored for motility. Because normal ciliary motility consists of an initiation of bending combined with propagation of the initial bend down the length of the axoneme (Brokaw, 1994), we scored only initiation of bending as a criterion for motility since cilia on K2.4-injected embryos are perhaps too short to exhibit propagation of bending. Specifically, if the first 3 μm of cilium above the blastomere surface showed a 10° change of angle or more from one apogee to the other, then this cilium was defined as "initiating a ciliary bend" and was scored as "motile." Thus, a cilium was considered motile even if it did not propagate the initiated bend, as is the case for most long apical tuft cilia of the animal pole. By conservatively defining motility as a function of bend initiation, we restrict those cilia described as being "immotile" to those cilia that remain exceptionally still. Control cilia typically initiate a ciliary wave by bending at the base through almost 90°.

Length and Density of Cilia on Blastula Surface. To collect data for determination of "Average length of cilia" and "Density of cilia" (see Tables II and III), dozens of cilia were visualized simultaneously by video-enhanced differential interference contrast microscopy of the bottom face of embryos compressed gently against the coverslip in the injection chamber. The cilia were trapped in this region and held still in a single focal plane by the embryo's surface. All cilia whose full length was visible in a single focal plane in these en face regions were traced onto a plastic transparency. Cilia that passed out of the focal plane were clearly distinguished at the periphery of this flattened face by changing focus. Ciliary bases were distinguished from ciliary tips by a broadening of the base visible at the blastomere's surface. For cilia where the entire length was not clearly visible, its base was marked on the transparency with a dot. To generate more length measurements and to ensure that ciliary length data were not biased by sampling only cilia trapped at the embryo surface, cilia lengths were also traced at the embryo equatorial regions described above. Equatorial video footage was viewed frame by frame until a single cilium's entire length, from base to tip, appeared in focus in a single video frame, at which point its full length was traced. The accuracy of this method in reproducibly capturing the full length of a cilium was confirmed by repeatedly tracing cilia that appeared in focus multiple times.

To determine "Average length of cilia," lengths of traced cilia were measured in millimeters on the transparencies and then converted to micrometers from calibrations of the image dimensions using recorded images of a stage micrometer. To produce an average length for cilia sampled from the entire embryo surface, measurements of cilia from equatorial and en face traces were pooled.

We observed nonnormal distributions of length measurements, so to statistically compare the ciliary length difference between K2.4-injected and control embryos, we performed a Krustal–Wallis test for nonparametric analysis of variance (Zar, 1984) rather than a single factor analysis of variance. By the Krustal–Wallis test, the lengths of cilia on K2.4-injected, SUK-4–injected, nonspecific IgG, and uninjected embryos were found to be highly significantly different (test statistic, H_c, = 171.048; critical value for H = 16.266 at α = 0.001). To determine which mean ciliary lengths were significantly different from the others, we used a nonparametric multiple comparison test similar to the Tukey test (Zar, 1984) but which does not assume population normality or homogeneity of variance. We performed nonparametric multiple comparisons of ciliary lengths by ranking the ciliary lengths and sequentially comparing each condition with the others from the largest difference to the least. We thereby determined that a highly significant difference (α = 0.005) exists between the lengths of cilia on K2.4-injected embryos and every control condition (test statistic, Q, = 12.7552 between K2.4-injected and uninjected embryos; 7.3038 between K2.4-injected and SUK-4–injected embryos; 5.8066 between K2.4-injected and nonspecific IgG-injected; critical value for $Q_{0.005,4}$ = 3.342). Such a difference does not exist between the control conditions (Q = 3.1771 between nonspecific IgG–injected and uninjected embryos; 1.5182 between SUK-4–injected and uninjected embryos; 1.3095 between SUK-4–injected and nonspecific IgG-injected embryos).

The "Density of cilia" values were determined from the en face traces as follows. After marking the bases of every cilium visible on the flattened embryo face with a dot on the embryo trace, an irregular polyhedron was drawn connecting the most peripheral dots. In cases where large inclusions (such as the injected oil droplet) obscured a region of the embryo face, a polyhedron was drawn between the most peripheral dots so as to exclude the inclusion from the circumscribed area. The number of ciliary bases circumscribed by the polyhedron, including bases at the polyhedron corners, were counted. To determine the area of the circumscribed polyhedron, a grid of 1-cm^2 squares was overlaid on it so that the longest side of the polyhedron aligned with a gridline and so the dot at one end of that polyhedron side sat atop an intersection point (vertex) on the grid. With the longest side of the polyhedron away from the scorer, each grid vertex was designated as representing the 1 cm^2 above it and to its left. The total number of grid vertices within the polyhedron was counted, and any vertex that fell on the polyhedron boundary line was counted if the 1 cm^2 above it and to its left was within the polyhedron. The total number of grid vertices circumscribed by the polyhedron therefore represented the total number of centimeters squared circumscribed by the polyhedron and was converted to micrometers squared from calibrations of the image dimensions using recorded images of a stage micrometer. Dividing the pooled total number of circumscribed ciliary bases by the pooled total number of circumscribed micrometers squared and multiplying by 100 produced the Density of cilia per 100 μm^2 values in Table II. We used density per 100 μm^2 because at ciliogenesis, 100 μm^2 was the apparent apical surface area of one blastomere.

Electron Microscopic Analysis of Axonemes on Injected Blastulae

After microinjection, sea urchin embryos were transferred one by one to separate wells of an observation chamber where their development could be monitored through the time when uninjected control embryos withdrawn from the same injection chamber were ciliated and swimming vigorously. After confirming that all cilia on the K2.4-injected embryos were completely paralyzed, injected embryos were withdrawn individually from the observation chamber and transferred to fixation buffer. Control embryos received identical treatment and processing. Embryos were prepared for EM using a procedure modified from Masuda and Sato (1984) after several other protocols produced either poor ciliary morphology as seen in the light microscope, or inadequate fixation as seen in the electron microscope. Although this protocol uses detergent in the fixation step producing demembranated axonemes attached to the embryo surface, the axonemes remained intact and provided consistently better preserved ultrastructure than other fixations attempted. Ciliated blastulae were fixed for 1 h in 2.5% glutaraldehyde, 0.1 M Pipes, pH 8, 0.8 M glycerol, 0.01 M EGTA, 2 mM $MgSO_4$, and 1% saponin; washed three times in 0.1 M Pipes, pH 8.0, 0.8 M glycerol, 1 mM EGTA, 0.5 mM $MgSO_4$; treated for 1 h in the same buffer containing 0.2% tannic acid; washed three times in 0.1 M Pipes, pH 8, 0.8 M glycerol, 0.5 mM $MgSO_4$; postfixed for 1 h in 1% OsO_4, 0.1 M phosphate buffer, pH 8, 0.3 M sucrose; and finally washed in 0.1 M phosphate buffer, pH 8, 0.3 M sucrose. All steps were performed at 25°C. The embryos were dehydrated through an acetone series that included 1 h in 2% uranyl acetate in 70% acetone and were flat-embedded in Embed-812 (Electron Microscopy Sciences, Fort Washington, PA). 60–70-nm sections were cut and stained with uranyl acetate and lead citrate and then imaged on an electron microscope (Model 410; Phillips Electronic Instruments, Co., Mahwah, NJ) operated at 80 kV.

To quantitate the frequency of occurrence of central pair apparati in cross and oblique sections of ciliary axonemes by EM, we only scored axonemes in which outer doublets were distinct. For cross sections, axonemes were scored as having a central pair when nine outer doublet MTs could be localized at the same time that 20-nm-diam rings or circles could be localized in the axoneme interior (for example, Fig. 6 *E*). Axonemes were scored as having centralized amorphous material, but no recognizable central pair, when no central 20-nm-diam rings or circles were observed in the axoneme interior but electron-dense material still appeared focused at the center of the cavity (for example, Fig. 6, *G* and *H*). Axonemes were scored as completely lacking central pairs when neither 20-nm rings or circles nor centralized amorphous material was observed (for example, Fig. 6 *F*). In addition, oblique sections (which cut completely across the axoneme) were scored, while longitudinal sections were not, to avoid incorrectly scoring any grazing sections that did not cut into the central pair. For oblique sections, axonemes were scored as having a central pair when linear walls of any central pair MT were visible in the central

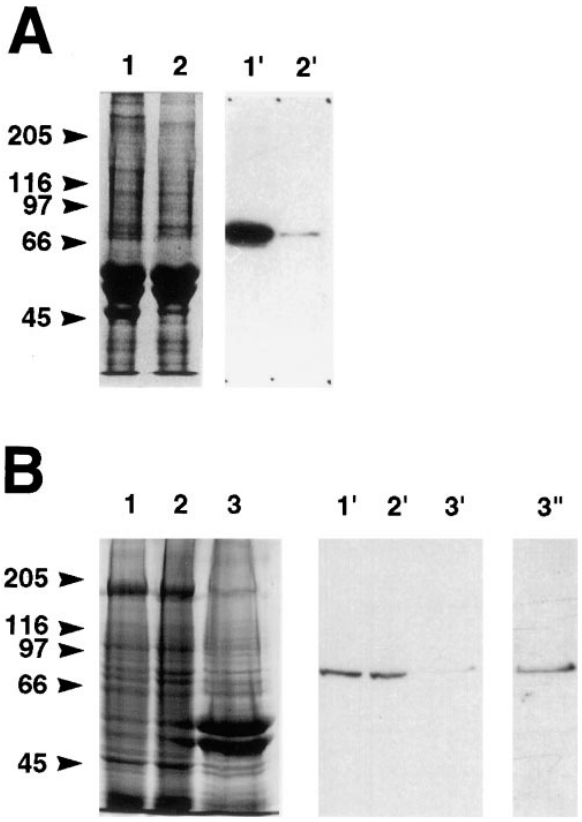

Figure 1. Specificity of K2.4 anti–kinesin-II antibody. (*A*) Coomassie blue–stained gel of MTs polymerized and pelleted in the presence of AMP-PNP from *S. purpuratus* cytosol (lane *1*) or in the presence of ATP (lane *2*). An identical gel was transferred to nitrocellulose and then probed with K2.4 to show that the antibody recognizes the 85-kD $SpKRP_{85}$ subunit of kinesin-II and follows the kinesin-II as it pellets with microtubules in the presence of AMP-PNP (lane *1′*) but not appreciably in the presence of ATP (lane *2′*). (*B*) Coomassie blue–stained gel of whole *L. pictus* ciliated blastulae (lane *1*), deciliated blastulae (lane *2*), and isolated cilia (lane *3*) shown loaded at 100 μg per lane. An identical gel was transferred to nitrocellulose and then probed with K2.4 to show that the antibody strongly and specifically recognizes the 85-kD subunit of kinesin-II in *L. pictus* whole blastulae (lane *1′*) and deciliated blastulae (lane *2′*). K2.4 also detects KRP_{85} in isolated cilia (lane *3′*) but at a much lower level (5–10% by weight total protein) than in embryos. Increasing the exposure time for the enhanced chemiluminescence–detected blot from 4 min (lanes *1′*, *2′*, and *3′*) to 20 min (lane *3′′*) clearly reveals the KRP_{85} band in cilia during the embryonic stage at which K2.4 exerted its inhibitory effect.

density. Data were derived from 21 cross or oblique sections from 4 control embryos, and 39 cross or oblique sections from 5 K2.4-injected embryos.

Results

Characterization of Antibodies and Detection of Ciliary Kinesin-II by Immunoblotting

The experimental monoclonal anti–kinesin-II antibody used in the microinjection experiments described here, K2.4, was generated against purified *Strongylocentrotus purpuratus* kinesin-II and shown to react specifically with the AMP-PNP–enhanced, ATP-sensitive MT-binding $SpKRP_{85}$ subunit of *S. purpuratus* kinesin-II (Fig. 1 *A*; Cole et al., 1993; Henson et al., 1995). To ensure that K2.4 reacts specifically with kinesin-II in the *Lytechinus pictus* embryos that were used in these microinjection studies at the stage where its inhibitory effect was observed (below), we probed whole *L. pictus* blastula-stage embryos (before and after deciliation) and isolated cilia (Stephens, 1986) with K2.4. We observed a strong, specific reaction with $SpKRP_{85}$ in blastulae before and after deciliation and a fainter reaction with cilia (Fig. 1 *B*), indicating first that K2.4 is specific for kinesin-II in *L. pictus* blastulae, and second that the majority of the kinesin-II is stockpiled in the blastula cell bodies with a small fraction being present in cilia. Blot densitometry indicated that cilia contain between 5–10% as much kinesin-II per milligram total protein as is contained in cell bodies.

The three controls for the microinjection of anti–kinesin-II monoclonal antibodies were uninjected embryos, embryos injected with a nonspecific mouse IgG, and embryos injected with the antikinesin mAb SUK-4, which is the same isotype as K2.4, binds *L. pictus* kinesin, blocks kinesin motor function in vitro (Ingold et al., 1988; Wright et al., 1991, 1993), and blocks the delivery of exocytic vesicles to the plasma membrane (Steinhardt et al., 1994; Bi et al., 1997).

Lack of Effect of Anti–kinesin-II Antibody Microinjection on Mitosis and Cell Division

Kinesin-II immunolocalizes to punctate, vesicle-like structures in sea urchin embryonic mitotic spindles, suggesting that it might participate in mitosis or cell division (Henson et al., 1995). To investigate this possibility, we examined experimental and control embryos for effects on progression through mitosis and cytokinesis during cleavage-stage development (Fig. 2). We observed that embryonic cells containing anti–kinesin-II mAbs displayed identical average cell cycle duration to the uninjected controls and no significant difference from nonspecific antibody-injected controls (Fig. 2, Table I). This result did not support the hypothesis that kinesin-II has an essential function in mitosis or cell division.

Effects of Anti–kinesin-II Antibody Microinjection on Ciliogenesis

Kinesin-II immunolocalizes to punctate, detergent-insensitive particles in flagellar axonemes, and with basal body–like structures in the sperm midpiece (Henson et al., 1997), suggesting that it might participate in axoneme assembly or function. In support of this hypothesis, we observed that the microinjection of anti–kinesin-II mAbs produced a dramatic inhibition of the assembly of motile cilia on blastula stage embryos. An obvious consequence of this effect was that K2.4-injected embryos remained stationary in the injection chamber indefinitely, while uninjected or control-injected embryos formed normal motile cilia with which they swam around in the sea water of the injection chamber (Fig. 2, *final panel*; Table I).

Visual examination of the surfaces of K2.4-injected embryos revealed that the embryos' inability to swim resulted from defects in ciliogenesis leading to the presence of

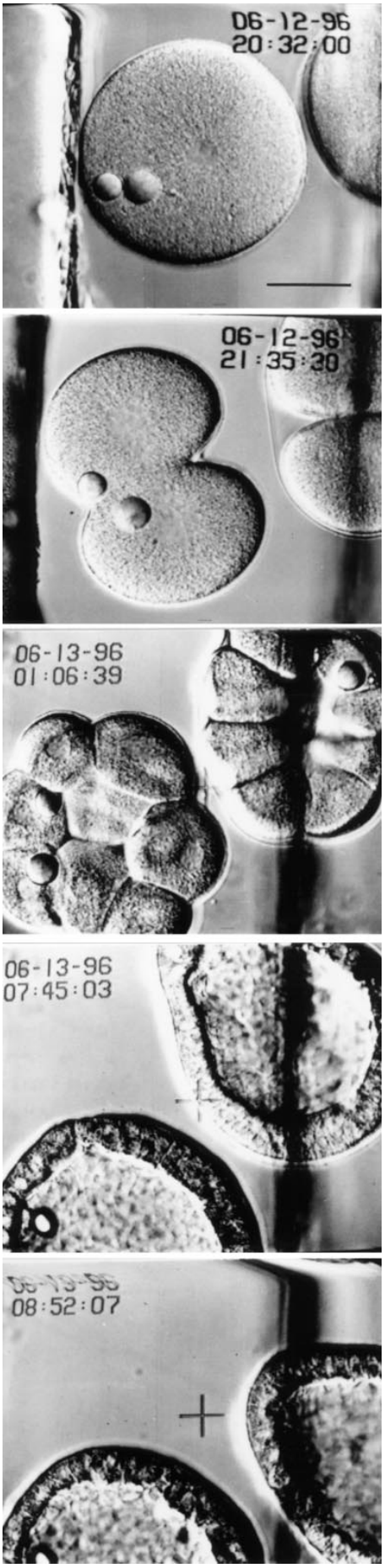

Table I. Quantitation of Cell Cycle Duration and Embryo Swimming in K2.4-injected, Control-injected, and Uninjected Embryos

	Average duration of cell division cycle	Percent blastulae swimming
	h:min ± SD	
K2.4-injected	1:02 ± 0:15	0 (n = 33)
SUK-4–injected	0:59 ± 0:10	100
Nonspecific IgG–injected	ND	100
Uninjected	1:02 ± 0:16	100

To determine the average duration of cell division cycles, progression through the fourth through seventh cell division cycles were measured and averaged for four K2.4-injected embryos, three SUK-4–injected embryos, and two uninjected embryos monitored simultaneously in a single batch of fertilized eggs in a single injection chamber, as described in Materials and Methods. The percentage of blastulae swimming for K2.4-injected embryos was obtained by monitoring 33 K2.4-injected embryos that remained stationary indefinitely, while control-injected and uninjected embryos in the same injection chamber were swimming. In fact, all control embryos that reached the ciliated blastulae stage ($n > 100$) swam, but none of the K2.4-injected embryos did so.

short, completely paralyzed cilia on the blastula surface (Fig. 3). Thus, high magnification observations of the surfaces of swimming control blastulae revealed the presence of long beating cilia, whereas the anti–kinesin-II–injected embryos possessed equal numbers of very short, immotile cilia over their outer surfaces (Fig. 3). The effects of anti–kinesin-II antibody microinjection on ciliogenesis were quantitated in detail (Table II). This analysis revealed that virtually all cilia on the K2.4-injected embryos were completely immotile, and they averaged typically less than half the length of cilia on control embryos (7.3 μm long versus 12–17 μm long for controls; Table II). When analyzed statistically as described under Materials and Methods, ciliary lengths on K2.4-injected embryos were highly significantly different than all three control conditions, while the control conditions were not highly significantly different from each other. In addition, the short cilia on the anti–kinesin-II–injected blastulae all had a conspicuous, knoblike bulb at their distal tips, apparently irrespective of the length or age of the cilium (Fig. 3 *C*). These knobs were found at the tips of virtually all the K2.4-injected cilia, where they remained stationary and stable, but they were exceedingly rare on control cilia.

The simplest interpretation of these results is that the microinjection of the anti–kinesin-II antibody interferes with the assembly of motile cilia. However, it could be argued that the short ciliary lengths observed in K2.4-

Figure 2. Effect of K2.4 anti–kinesin-II antibody microinjection on mitosis and cell division. This series of video frames illustrates the development of two *L. pictus* embryos, one microinjected with K2.4 (*left embryo*) and the other with SUK-4 (*right embryo*), through the swimming blastula stage. These two embryos were fertilized at 19:40, injected at 20:12, and as revealed by the recorded time/date stamps, are pictured here at 0:52, 1:55, 5:26, 8:05, and 13:12 h after fertilization. In the final frame, the SUK-4–injected embryo on the right starts to swim out of the injection chamber and into the sea water, leaving the stationary K2.4-injected embryo behind. The intracellular oil droplets confirm that these embryos were successfully injected. The dark vertical lines are the edges of the microinjection chamber. Bar, 40 μm.

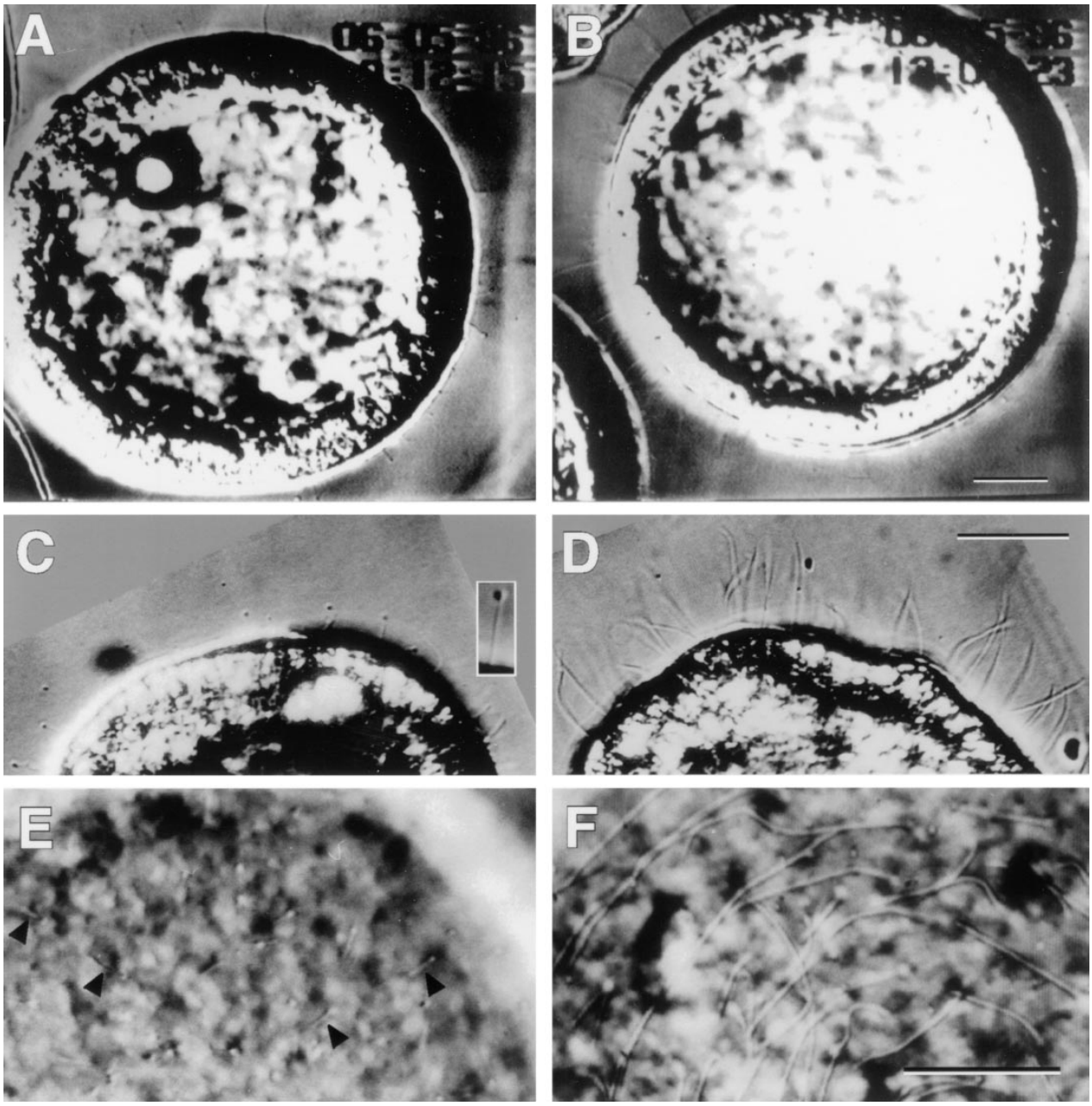

Figure 3. Effect of K2.4 anti–kinesin-II antibody microinjection on ciliogenesis during sea urchin development. Images of live embryos (*A* and *B*) show that an embryo injected with K2.4 at the one-cell stage (*A*) develops to the swimming blastula stage, but only forms short, paralyzed cilia, while an uninjected embryo (*B*) undergoes normal ciliogenesis and forms long, rapidly beating cilia over its entire surface. Differences in ciliary length are more easily seen in embryos fixed in 3% glutaraldehyde in calcium-free sea water (*C* and *D*), where the short paralyzed cilia with knoblike structures at the tips (*C*, *inset*) are seen on a K2.4-injected embryo (*C*), while an uninjected control embryo (*D*) possesses long cilia without terminal knobs. High-magnification images of the embryo surface juxtaposed to the coverslip on K2.4-injected and control embryos (*E* and *F*) show the different lengths, but similar density per unit area, of cilia on K2.4-injected embryos (*E*) and on uninjected (*F*) embryos. Four of the short cilia on the K2.4-injected embryo pictured (*E*) are indicated with arrowheads. Image pairs (*A* and *B*, *C* and *D*, and *E* and *F*) are shown at the same scale. The cilium in *C*, *inset* was 11 μm long. Bars, 20 μm.

injected embryos is an artifact resulting from fortuitously measuring ciliary lengths at the start of the 60-min-long cell cycle (Table I) when ciliogenesis has just begun; cilia measured at this time would obviously be transiently shorter than normal because of the timing of the measurements of ciliary lengths. To rule this out, we analyzed cilia on the same embryos at two different time points, 40 min apart (Table III), and observed that the average ciliary length in K2.4-injected blastulae plateaus at a short value, suggesting that the short ciliary length on K2.4-injected embryos represents an "end point" that does not change significantly over subsequent time. The fact that the density of cilia per unit area increases significantly between these observation times (Table III) confirms that the blas-

Table II. Quantitation of Ciliary Motility, Length, and Number in K2.4-injected Control-injected, and Uninjected Embryos

	Percent cilia motile (*n*)	Average length of cilia (*n*)	Density of cilia (*n*)
		μm	*per 100 μm²*
K2.4-injected	0.6 (170, 7)	7.3 (214, 7)	1.1 (70, 2)
SUK-4–injected	98.5 (130, 4)	14.4 (73, 4)	ND
Nonspecific IgG–injected	93.0 (71, 2)	12.4 (76, 2)	0.88 (83, 2)
Uninjected	95.0 (218, 7)	16.4 (240, 7)	0.99 (171, 3)

Sample sizes (*n*) included in parentheses in the table are the number of cilia scored, number of embryos analyzed. Criteria scoring a cilium as motile for the determination of "Percent cilia motile" are described in Materials and Methods.

tomeres were continuing to divide while the average ciliary length had reached a plateau.

Effects of Anti–kinesin-II Antibody Microinjection into One Cell of a Two-Cell Embryo

To control for potential differences in the response to microinjection between individual embryos, we injected one cell of a two-cell embryo with the anti–kinesin-II antibody (Fig. 4). Remarkably, the resulting blastula was covered on the side derived from the K2.4-injected blastomere with shortened, paralyzed cilia, and on the other, uninjected side with normal, beating cilia. These "half-paralyzed" blastulae did indeed swim, with the motile half pulling the paralyzed half around the injection chamber, and on these embryos, normal, motile cilia beat side-by-side with paralyzed cilia on adjacent blastomeres. Thus, individual K2.4-injected blastomeres fail to assemble normal cilia, while adjacent blastomeres ciliate normally.

Table III. Quantitation of Ciliary Length and Density at Two Different Time Points on a Region of the Surface of Anti–kinesin-II–injected, Control Antibody–injected, and Uninjected Embryos

	Average length of cilia		Density of cilia	
	μm		*per 100 μm²*	
	First observation	Second observation	First observation	Second observation
K2.4-injected	6.0 (46)	5.5 (55)	1.14 (70)	1.56 (71)
Nonspecific IgG–injected	11.9 (50)	10.6 (39)	0.88 (83)	1.05 (44)
Uninjected	13.9 (140)	17.4 (61)	0.99 (171)	1.17 (62)

Cilia lengths and densities per unit area were measured on the surface of two K2.4-injected blastulae, two nonspecific IgG-injected blastulae, and three uninjected blastulae to generate the "First observation" data. To generate "Second observation" data, cilia lengths and densities were measured again, 40 min later, on exactly the same surface region of the first embryo in each condition. Number of cilia scored are included in parentheses (*n*) in the table.

Ciliary Length Distributions on Control versus Anti–kinesin-II–Injected Embryos

Cilia on anti–kinesin-II–microinjected embryos were homogeneously short with an average length that was twofold shorter than that of control embryos at the same stage (Table II). Control embryos not only possessed longer cilia than K2.4-injected embryos, but in addition, the ciliary lengths on control embryos were heterogeneous, with cilia at the animal pole normally growing to three times the length of cilia on the rest of the embryo (Burns, 1973, 1979). Significantly, in analyzing the length distributions on control embryos, we observed a discrete subpopulation

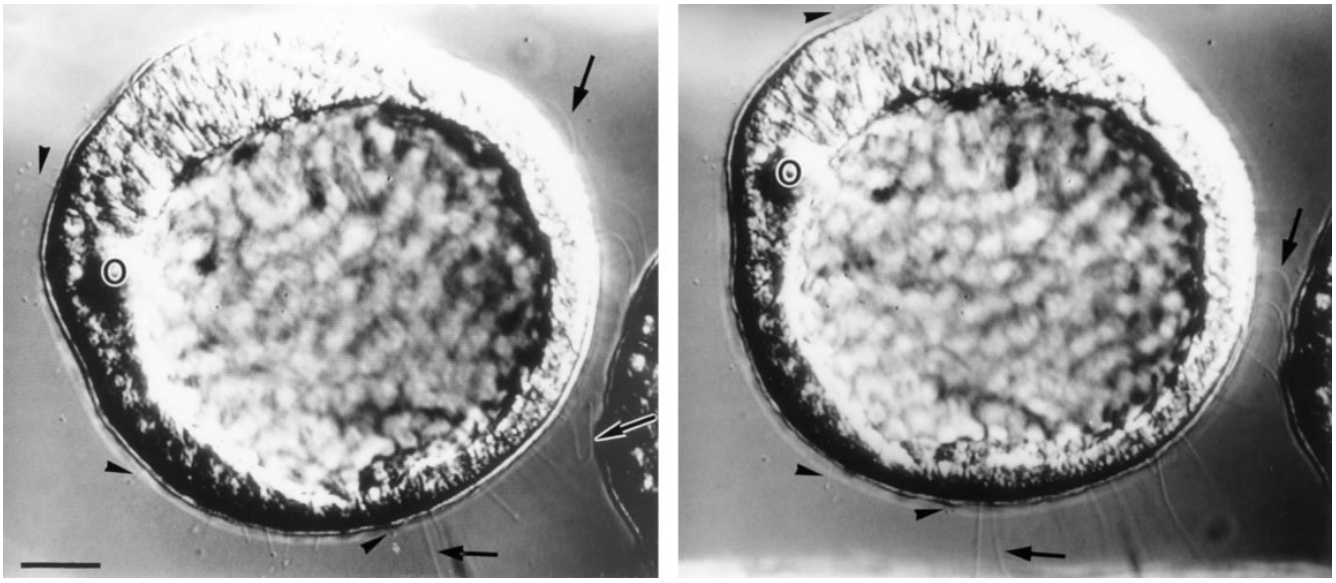

Figure 4. Two views of a half-paralyzed chimeric blastula resulting from the microinjection of one cell of a two-cell embryo with the K2.4 anti–kinesin-II antibody. The oil droplet (*O*) marks the injected half of the embryo on the left side of these video-enhanced contrast images, where many short, immotile cilia are clearly visible (*arrowheads*). In contrast, many long, motile cilia (*arrows*) are visible on the uninjected, control, right half of the blastula. The embryo has spun clockwise between these two images taken ~5 s apart, driven by its long motile cilia, which are most clear when their movements are impeded by the adjacent unciliated embryo (*lower right* of each image) or by the wall of the injection chamber (*bottom*). The close proximity of short paralyzed cilia to long motile cilia is apparent at the bottom of these images. Bar, 20 μm.

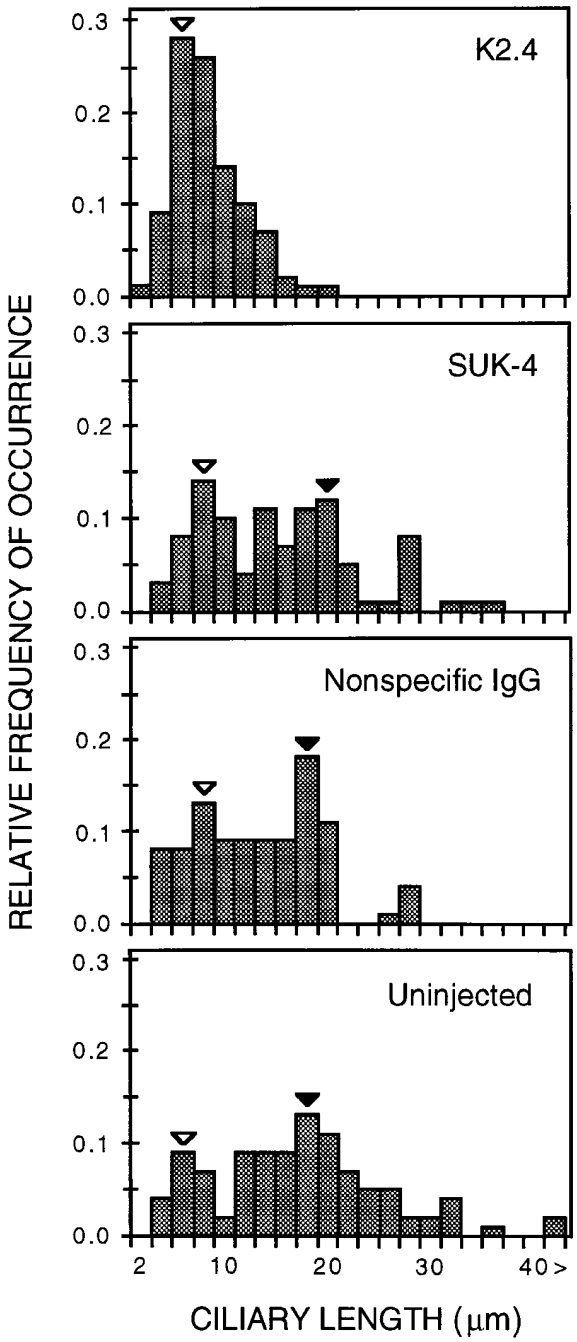

Figure 5. Relative frequency of occurrence of different lengths of cilia in K2.4-injected and control SUK4-injected, nonspecific Ig–injected, and uninjected embryos. Relative frequencies were determined by pooling individual cilia length measurements from all cells at each condition and dividing the number of cilia in each length bin by the total number of cilia measured for length. Cilia were binned such that the 2-μm bin contains cilia of length 1.00–2.99 μm, the 4-μm bin contains cilia of length 3.00 to 4.99 μm, etc. Data are derived from 214 cilia on seven K2.4-injected embryos, 73 cilia on four SUK-4–injected embryos, 76 cilia from two nonspecific IgG–injected embryos, and 246 cilia on seven uninjected embryos. Open arrowheads indicate the mode of short cilia present on all embryos, whereas closed arrowheads indicate the major mode of normal length cilia that are present on control but not on K2.4-injected embryos.

of cilia whose average length corresponds to that of the short cilia on K2.4-injected embryos.

To investigate these patterns of recurring ciliary lengths in detail, we analyzed the entire pool of length data as length distribution histograms (Fig. 5). The lengths of cilia from the anti–kinesin-II–injected embryos are all clustered into a positively skewed distribution with a single mode at ~7 μm of length (Fig. 5, *upper panel*) and with only 20% of the cilia 11 μm or longer. However, ciliary lengths from the control blastulae are spread over a much wider distribution of longer lengths than cilia from K2.4-injected blastulae, with between 62 and 78% of cilia 11 μm or longer, and they appear to fall into three subpopulations that differ in their modal length. One subpopulation of cilia has a predominant mode at ~18 μm. A second subpopulation of control cilia displays a prominent mode at 7 μm, which is coincident with the mode of the short cilia on anti–kinesin-II–injected embryos. In addition, another subpopulation of cilia on control blastulae appears to constitute a minor third mode at ~30 μm of length, but this group of longer cilia appears less discrete than those that are 18 and 7 μm long.

Ultrastructural Morphology of Axonemes on Control and Anti–kinesin-II–injected Embryos

The light microscope provided clear evidence that the cilia on K2.4-injected embryos were morphologically and behaviorally different from those on control embryos. To identify a potential ultrastructural basis for the ciliary paralysis, we developed a system for processing single embryos from microinjection through embedding for electron microscopy. Several methods of fixation of intact cilia were tried, including those used for *Chlamydomonas* flagella (Kozminski et al., 1993), but they resulted either in artifactual production of conspicuous knobs on distal tips of control cilia or in obscured axonemal structure. However, we found that a modified protocol of Masuda and Sato (1984) developed for sea urchin gave consistent preservation of axonemal architecture on the surface of intact blastulae. EM analysis of sections cut through the axonemes of paralyzed K2.4-injected embryos revealed that, although they contain nine outer doublet MTs, they completely lack central pair MTs (Fig. 6). This 9+0 structure of the paralyzed axonemes is in stark contrast to the clear 9+2 structure of the control embryo axonemes where the central pair and its associated structures are distinct (Fig. 6, *A*, *E*, and *J*). Paralyzed cilia also possessed amorphous material within and around the nine outer doublet MTs that sometimes appear disorganized (Fig. 6, *F–I*, and *K*). The lack of central pair MTs in paralyzed cilia is apparent in both cross (Fig. 6, *F–I*) and oblique (Fig. 6, *B*, *C*, and *K*) sections. Scoring 39 such sections revealed that none contained central pair microtubules: 54% completely lacked any ultrastructural feature in the center of the axoneme (e.g., Fig. 6, *F* and *K*), while the remaining 46% contained indistinct but still centralized amorphous material (e.g., Fig. 6, *G* and *H*). Sometimes the outer doublets collapsed inward as seen in an extreme case in Fig. 6 *I*, where the nine outer doublets appear to spiral into the axoneme's central cavity. In control axonemes, 86% of 21 scored sections possessed two distinct central pair MTs (Fig. 6 *E*),

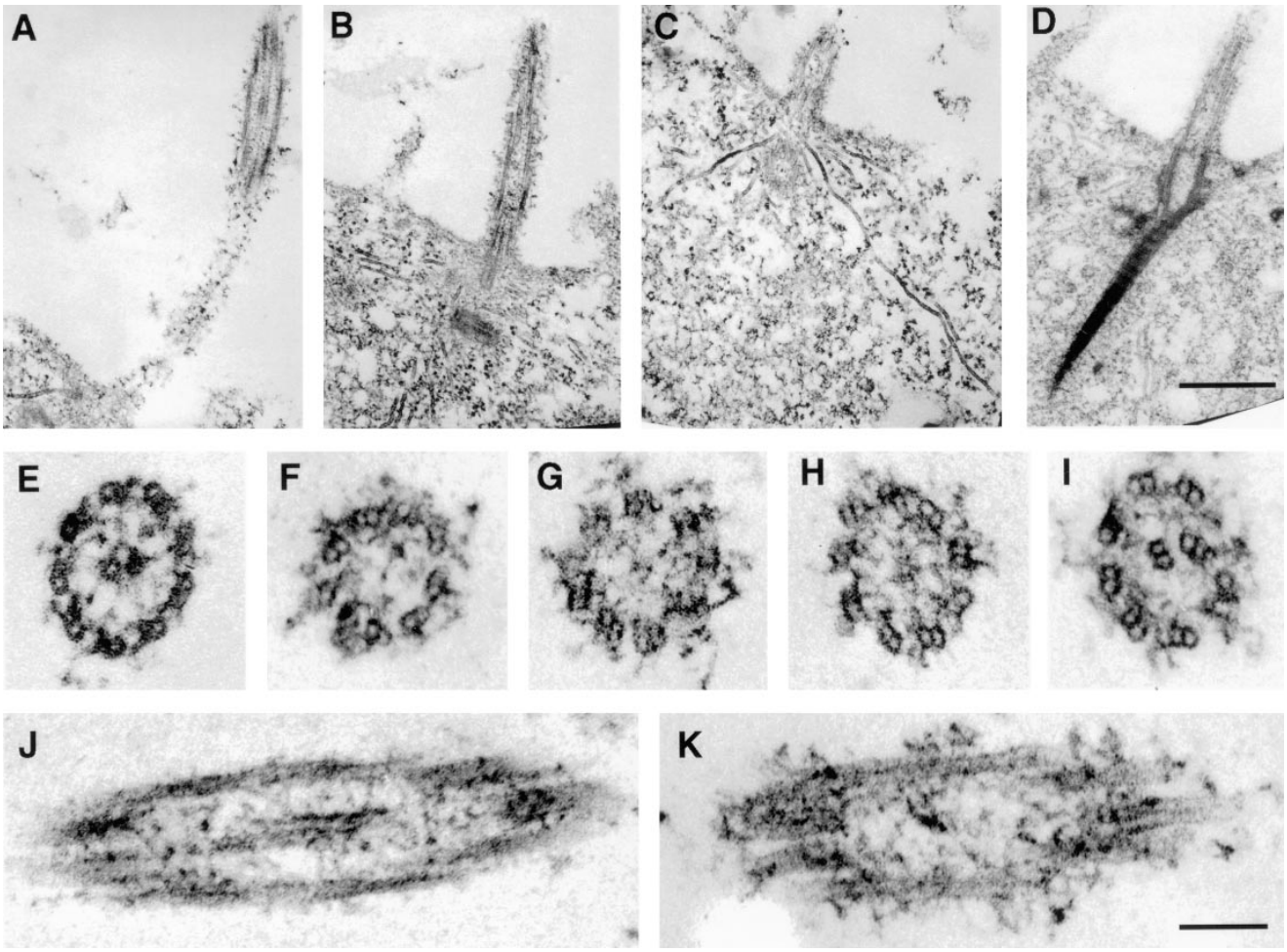

Figure 6. Electron micrographs of axonemes and basal body regions at the ciliated blastula stage in control (*A*, *E*, and *J*) and K2.4 anti–kinesin-II antibody-injected (*B–D*, *F–I*, and *K*) embryos. Images of the basal body regions of ciliated K2.4-injected embryo blastomeres reveal a normal arrangement of centrioles (*B*), radiating intracellular array of MTs (*C*), and striated rootlets (*D*). However, oblique sections across an axoneme on K2.4-injected embryos suggest an absence of central pair MTs (*B*) that are present in control axoneme oblique sections (*A*). Axonemal cross sections at higher magnification reveal that, while control axonemes present a typical arrangement of nine outer doublet MTs around a central pair of singlet MTs (*E*), axonemes from the paralyzed, K2.4-injected embryos completely lack central pair MTs and possess only the nine outer doublets (*F–I*). A pair of long oblique sections also reveals the clear difference between central pair presence in a control axoneme (*J*) and absence in an injected embryo axoneme (*K*). The panel of axoneme cross sections from K2.4-injected embryos (*F–I*) displays the variety of patterns of axonemal content exhibited in the absence of the central pair, including axonemes that appear devoid of either central pair or centralized amorphous material (*F*), axonemes with some centralized amorphous material (*G* and *H*), as well as axonemes where apparently all nine outer doublets can be counted as they spiral into the central cavity (*I*). Bars: (*A–D*) 500 nm; (*E–K*) 100 nm.

while the remaining 14% contained centralized material with a less distinct ultrastructure. These results suggest that kinesin-II is required for the assembly or maintenance of central pair singlet MTs. In contrast, and as suggested by the normal cilia density on the surface of paralyzed embryos (Table II), kinesin-II is apparently not required for the positioning of basal bodies or formation of singlet cytoplasmic MTs and striated rootlets which appeared indistinguishable from control in the anti–kinesin-II–microinjected cells (Fig. 6, *B–D*).

Specificity and Longevity of Anti–kinesin-II Antibody Effects on Ciliogenesis

To investigate the persistence of this effect on ciliogenesis, we monitored the development of anti–kinesin-II antibody–injected embryos for several days after control-injected and uninjected embryos had ciliated and begun to swim around in the injection chamber and surrounding sea water. After formation of their short, immotile cilia, anti–kinesin-II–injected embryos underwent mesenchymal cell ingression, gastrulation, and spiculogenesis at comparable times to the same developmental events occurring in uninjected embryos inhabiting the same injection chamber (Fig. 7). The only noticeable difference from controls at these later stages was that K2.4-injected embryos, unlike controls, underwent a gradual swelling and increase in blastocoel volume. But despite the continuation of many normal developmental events, the cilia on anti–kinesin-II–injected embryos never increased their length or motility. Instead, the K2.4-injected embryos perpetually retained short immotile cilia on their surfaces for several days of

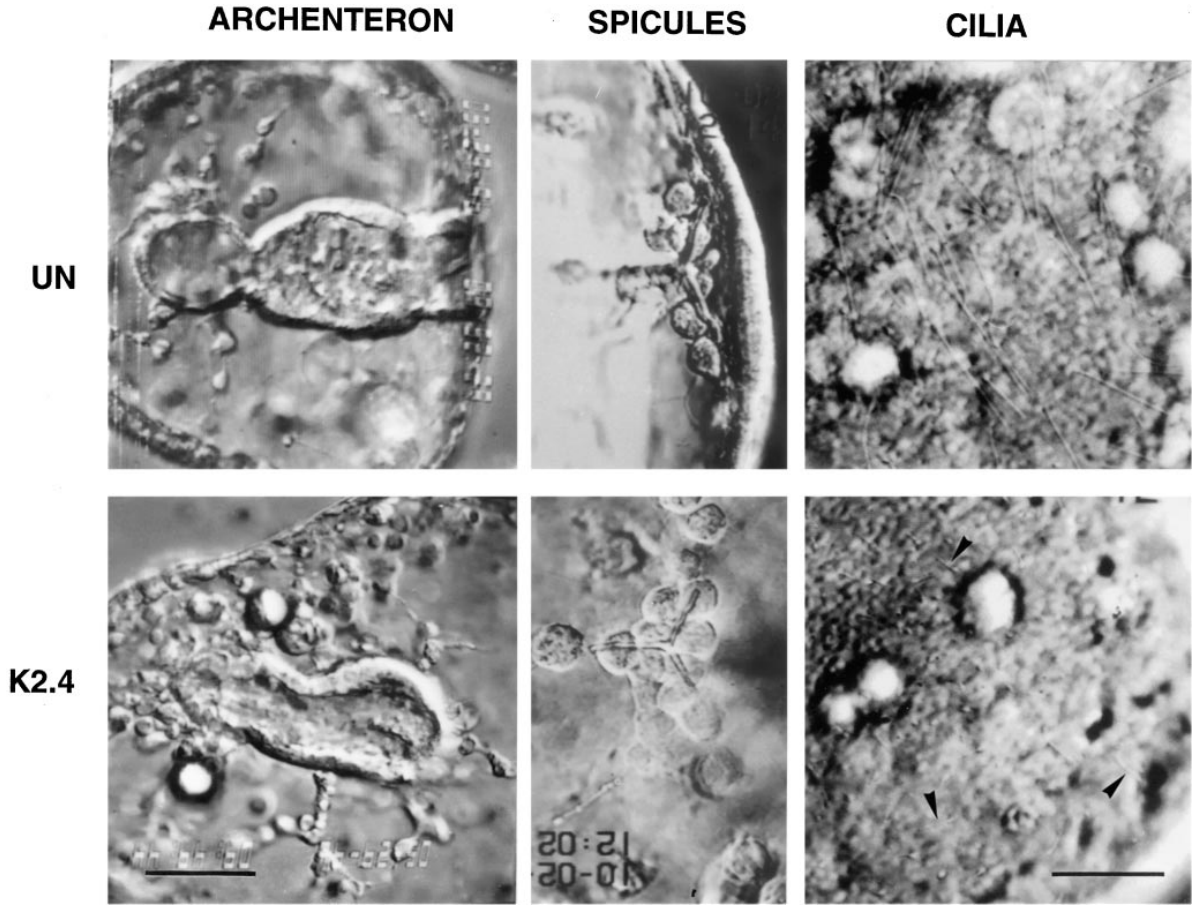

Figure 7. Effect of anti–kinesin-II antibody microinjection at one-cell stage on subsequent gastrulation and spiculogenesis. Gastrulation to form an archenteron (*left*) and formation of spicules (*middle*) occurred at similar times in uninjected (*UN*) and K2.4-injected (*K2.4*) embryos. Archenteron images are oriented with animal pole to the left; the blastopore of the K2.4-injected embryo faces toward the objective lens and lies out of the image plane. While control embryos continued to swim with their normal cilia (*right*), K2.4-injected embryos never grew normal length or motile cilia (*arrowheads*) during even the longest observation periods of >5 d. Archenteron is shown 4.5 d after fertilization and injection. In a separate batch of embryos, spicules and cilia are shown 1.5 d after fertilization and injection. Archenteron panels are same scale; spicule and cilia panels are same scale. Bars, 20 μm.

observation, indicating that the microinjection of anti–kinesin-II antibodies precluded normal ciliogenesis indefinitely.

Discussion

Kinesin-II Plays a Critical Role in Ciliogenesis in Sea Urchin Embryos

We have demonstrated that the microinjection of the anti–kinesin-II–specific mAb, K2.4, causes a dramatic inhibition of the formation of motile, 9+2 cilia of normal length on sea urchin blastula-stage embryos, suggesting that kinesin-II plays an important role in ciliogenesis. We demonstrated, by Western blotting, the presence of kinesin-II in whole blastulae, deciliated blastulae, and in isolated cilia, in which it is found at ~5–10% of the level in intact or deciliated blastulae (Fig. 1). To elucidate the function of kinesin-II in living sea urchin embryos, we microinjected the anti–kinesin-II antibody K2.4 into fertilized eggs and monitored their development by light microscopy. Although K2.4 injection had no apparent effect on mitosis or cytokinesis (Fig. 2), we observed a dramatic effect on ciliogenesis at the swimming blastula stage; cilia formed but were completely immotile and were consistently short compared to cilia on control embryos (Figs. 3–5). Histograms of ciliary length distributions revealed that the paralyzed cilia on K2.4-injected embryos fall into a single mode at 7 μm of length, coincident with the shortest of three modes seen for control embryo cilia (Fig. 5). This suggests that cilia on control embryos may progress through quantized assembly steps of which the first corresponds to the 7-μm length of the experimental cilia. Moreover, quantitation of the density of paralyzed cilia on the surface of K2.4-injected blastulae revealed similar densities to controls (Table II), suggesting that proper basal body localization was occurring in the absence of kinesin-II function. Therefore, we hypothesize that the dramatically shortened cilia resulted from defective assembly of the distal segment of cilia, so that in the absence of kinesin-II function, cilia achieved only the first of three discrete ciliary assembly states.

To investigate the ultrastructural basis for the paralysis of the cilia on K2.4-injected embryos, we analyzed individ-

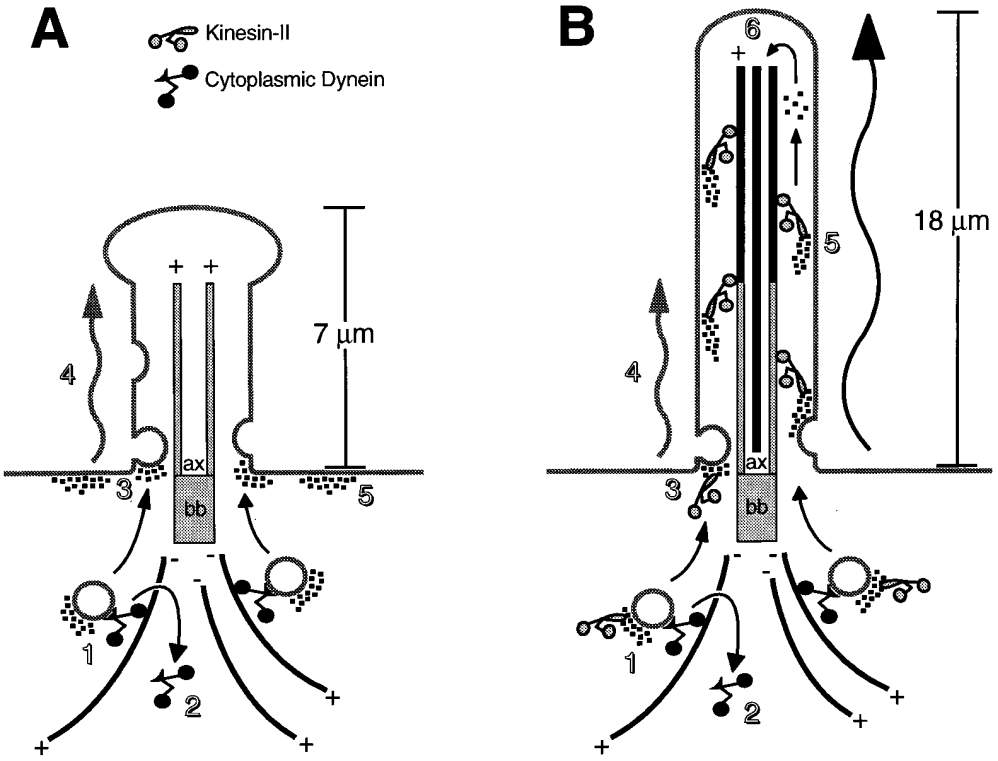

Figure 8. Model of role of kinesin-II during ciliogenesis in early sea urchin embryos. In the K2.4-injected embryos described in this study (*A*), basal bodies (*bb*) localize properly, and ciliary growth begins in the absence of kinesin-II function. An axoneme (*long gray rectangles* labeled *ax*) has formed, but it lacks components that confer motility and lacks a central pair. (*1*) Cytoplasmic dynein transports membrane vesicles (*gray circles*) and associated axonemal proteins (*black squares*) towards the minus ends of cytoplasmic MTs (*black lines*) located near the basal body. Upon arrival at the base of the cilium, cytoplasmic dynein may dissociate from the vesicles (*2*) as vesicles fuse with the plasma membrane at the ciliary base (*3*) delivering their membrane and associated proteins. But while vesicle delivery proceeds at a normal rate and required membrane can progress up the axoneme (*4*, *wavy gray arrow*), axonemal cargoes and their associated axonemal proteins can not proceed up into the axoneme toward the plus ends of the axonemal MTs without the activity of kinesin-II, and therefore they remain at the base of the cilium (*5*). The "procilium" that grows from this process is short (averaging 7 μm), perhaps because of the reduced delivery of axonemal structural proteins, immotile due to the absence of central pair MTs, and has a swelling at its distal tip perhaps because of disorganized or insufficient capping structures. In the control embryos (*B*), axonemal growth begins in much the same way as in K2.4-injected embryos, initially forming a 7-μm-long procilium assembly intermediate. Throughout axonemal growth, cytoplasmic dynein transports membrane vesicles and associated axonemal proteins including kinesin-II (*1*) to the base of the cilium. Upon arrival near the basal body, cytoplasmic dynein may dissociate from the vesicles (*2*) as the vesicles fuse with the plasma membrane (*3*) delivering membrane that can progress up the axoneme as needed (*4*). After rapid establishment of the 7-μm procilium (*gray*) by a mechanism not requiring kinesin-II function, elongation of the axoneme and assembly of central pair microtubules (*black*) is now supported by the activity of kinesin-II as it transports axonemal structural proteins or MT-stabilizing factors up the axoneme (*5*) toward the plus ends of the axonemal microtubules at the cilium tip. Ciliary growth (*wavy black arrow*), supported by kinesin-II–driven transport along the axoneme, produces a cilium that is both long (most often 18 μm) because of sufficient delivery of axonemal structural proteins (*6*) and motile because of the presence of an organized central pair. The bulbous swelling at the tip of the cilium is absent, perhaps because of sufficient delivery of ciliary cap structures and subsequent proper organization and stabilization of the axonemal tip.

ual microinjected embryos by electron microscopy. EM of axonemes on control and K2.4-injected embryos confirmed that the localization of basal bodies and the formation of associated cytoplasmic MTs and striated rootlets was occurring normally in K2.4-injected embryos (Fig. 6). Yet unexpectedly, and in striking contrast to the clear 9+2 structure of the control axonemes, axonemes on the surface of K2.4-injected embryos completely lacked central pair microtubules (Fig. 6). The paralyzed phenotype of the 9+0 cilia in the anti–kinesin-II–injected embryos may result from the absence of central pair MTs, like axonemes seen in many paralyzed *Chlamydomonas* mutants that have one or no central pair MTs (for review see Dutcher, 1995).

Thus, we propose a model (Fig. 8) in which ciliary growth in the sea urchin (Masuda, 1979; Masuda and Sato, 1984; Stephens, 1995) begins with formation of a short 7-μm-long assembly intermediate, or "procilium," which forms by a kinesin-II–independent pathway. We hypothesize that the plus end–directed kinesin-II motor (Cole et al., 1993) functions in the elongation of the 7-μm-long procilium and in establishment or stabilization of the central pair MTs, perhaps by transporting ciliary components outwards towards the assembling plus ends of axonemal MTs located at the distal ciliary tip (Euteneuer and McIntosh, 1981; Johnson and Rosenbaum, 1992).

Why Does Loss of Kinesin-II Function Result in Short and Paralyzed Cilia?

If, as we propose in our model, kinesin-II transports ciliary components along the axoneme to the ciliary tip for assembly, what could be the cargo of kinesin-II in sea urchin cilia whose absence would result in the formation of short and paralyzed 9+0 cilia? The short length of the cilia could arise if kinesin-II delivers structural or regulatory components required for the assembly or maintenance of the distal segment of the axoneme. Because the length of cilia is probably controlled by regulating the length of ax-

onemal MTs (Burns, 1973), perhaps the shortened phenotype that we observed resulted from insufficient delivery of tubulin (Johnson and Rosenbaum, 1992) or tektin-A (Linck and Langevin, 1982; Stephens, 1989; Norrander et al., 1995) to a site of assembly at the ciliary tips (Johnson and Rosenbaum, 1992). The ciliary paralysis we observed in kinesin-II–blocked embryos might result if one of its cargoes is axonemal dynein. This hypothesis is supported by studies showing that FLA10, a *Chlamydomonas* homologue of a kinesin-II subunit, delivers inner dynein arms to the growing ends of axonemes (Brokaw and Kamiya, 1987; Piperno and Ramanis, 1991; Piperno et al., 1996). Further work will be required to biochemically identify molecules missing in cilia formed on K2.4-injected embryos.

Because K2.4-injected sea urchin embryos form short but stable cilia, unlike the *Chlamydomonas fla10* mutant, which undergoes flagellar retraction at nonpermissive temperature (Kozminski et al., 1995), K2.4 injection of sea urchin embryos offers the potential opportunity to identify axonemal components targeted to cilia by kinesin-II at the ultrastructural level. This type of analysis has now revealed that axonemes on K2.4-injected embryos lack central pair MTs, which strongly suggests that ciliary components required for assembly or maintenance of the central pair MTs are potential cargoes of kinesin-II. Candidates include structural components of the central pair apparatus itself, such as the sea urchin homologue of the PF16 protein found on one central pair MT in *Chlamydomonas* (Smith and Lefebvre, 1996), or factors that stabilize the central pair, such as MT-capping proteins (Dentler, 1990; Miller et al., 1990). Sea urchin kinesin-II contains a large accessory subunit, $SpKAP_{115}$, that is localized at the presumptive cargo-binding carboxyl termini of the heterodimerized motor subunits (Wedaman et al., 1996), where it may function as an adaptor for cargo attachment (Cole et al., 1993; Wedaman et al., 1996). Interestingly, both $SpKAP_{115}$ and PF16 (Smith and Lefebvre, 1996) contain armadillo repeats, a protein motif proposed to mediate protein–protein interactions (Gindhart and Goldstein, 1996). It is therefore tempting to speculate that PF16 might be a component of kinesin-II's cargo by direct interaction.

Also of significance to this study is the observation that the *pf16* mutant exhibits a destabilized central pair MT that can be lost during preparation of axonemes (Smith and Lefebvre, 1996). This raises the possibility that the 9+0 axonemal structure we observe in the kinesin-II–blocked embryos may simply result from loss of an unstable central pair during fixation rather than from an inhibition of central pair formation. Although we can not formally rule out this possibility at this time, we favor the hypothesis that the cilia on K2.4-injected embryos never form a central pair because (*a*) not a single central MT was observed in K2.4-injected embryo axonemes and (*b*) several behavioral and morphological similarities are shared between the paralyzed cilia on living K2.4-injected blastulae before fixation and primary cilia in other cell types that are known to be 9+0 (Menco, 1980; Poole et al., 1985; Roth et al., 1987, 1988; Wheatley, 1995). Further work will be required to discriminate between inhibition of de novo assembly versus destabilization of central pair MTs in K2.4-injected embryos.

Loss of Kinesin-II Function Limits Ciliary Growth to a 7-μm Assembly Intermediate, a "Procilium," that Resembles a Primary Cilium

We believe that the three modes in the control cilia length distribution histogram (Fig. 5) represent three discrete ciliary assembly states; cilia form initially as (*a*) the 7-μm procilia, which quickly mature and grow to become (*b*) the 18-μm-long fully assembled and beating cilia, of which only the ones at the very animal pole will continue growing to become (*c*) the 30-μm-long cilia of the "apical tuft." The apparent entrapment of nascent cilia into the first assembly state by the inhibition of kinesin-II function raises interesting experimental predictions. First, the positively skewed distribution of cilia lengths on the K2.4-injected embryos (Fig. 5), with far more cilia of 7–8 μm than 1–2 μm, suggests that, in the absence of kinesin-II function, assembly of these 9+0 cilia to a length of 7 μm is somehow favored over shorter lengths. Further investigation will be necessary to test this hypothesis and to test its implication that short, 9+0 procilia may be found on normal, control blastulae. Initial formation of an immotile procilium could explain the observation that, in some urchin species, a minimum ciliary length is required before ciliary beating commences (Masuda and Sato, 1984).

In addition to their 9+0 axonemal core, the short and paralyzed cilia of the anti–kinesin-II–injected embryos share some interesting morphological similarities with primary cilia found on a variety of cell types (Menco, 1980; Poole et al., 1985; Roth et al., 1988; Wheatley, 1995; Wheatley et al., 1996). Primary cilia are also immotile (Sorokin, 1968; Roth et al., 1988), and in some epithelial cell lines up to a quarter of the cilia display varicosities very similar to the swellings that we observe on the tips of the K2.4-injected cilia (Fig. 3). The ultrastructure of the swellings on cilia of anti–kinesin-II–injected embryos was not revealed by our EM studies but will remain a goal of future work. Others have attributed the swellings on primary cilia of epithelial cells to the abnormal assembly of the primary ciliary axoneme (Jensen et al., 1987; Roth et al., 1988), as appears to be the case with the short cilia that grow on anti–kinesin-II–injected sea urchin embryos described here. In the light of these results, it will be interesting to determine if cells containing primary cilia lack functional kinesin-II.

Functions of Close Relatives of Kinesin-II in Other Systems

How does the proposed function of kinesin-II in sea urchin embryonic ciliogenesis relate to studies of its close relatives in other organisms? Homologues of the motor subunits of kinesin-II have been found in *Drosophila melanogaster, Caenorhabditis elegans*, fish, mouse, frog, and *Chlamydomonas rheinhardtii*, where they are implicated in axonal transport, pigment granule dispersion, and flagellar assembly (Aizawa et al., 1992; Kondo et al., 1994; Pesavento et al., 1994; Walther et al., 1994; Kozminski et al., 1995; Tabish et al., 1995; Yamazaki et al., 1995; Beech et al., 1996; Cole and Rosenbaum, 1996; Rogers et al., 1997; for review see Scholey, 1996). These proteins are members of a family of motors named the hetero-kinesins (Vale and Fletterick, 1997). The microinjection of K2.4

produces a phenocopy most similar to mutations in the *Chlamydomonas* FLA10 gene, which encodes a homologue of a subunit of kinesin-II (Rashid et al., 1995). The *fla10* mutation in *C. rheinhardtii* causes defects in flagellar assembly and stability (Lux and Dutcher, 1991). The FLA10-kinesin is concentrated in cell bodies relative to flagella and localized with centrioles, mitotic spindles, basal bodies, and axonemes (Vashishtha et al., 1996). These results, combined with our previous immunolocalization results (Henson et al., 1995, 1997) and our identification of kinesin-II in sea urchin cilia at 5–10% of the level found in cell bodies, are consistent with the hypothesis that kinesin-II is stockpiled in cell bodies with a fraction moving out along the axoneme to deliver components that are required for ciliogenesis. Furthermore, recent biochemical studies show that the FLA10-kinesin is also a subunit of a heterotrimeric motor complex (Cole and Rosenbaum, 1996) that is thought to drive the intraflagellar transport of 16S cargo complexes (Cole and Rosenbaum, 1996; Piperno and Mead, 1997), which form rafts beneath the flagellar membrane (Kozminski et al., 1993, 1995). Thus, work on the FLA10-kinesin together with our studies on kinesin-II provides a nicely consistent picture of a family of heterotrimeric kinesins playing important roles in axonemal assembly and stability in different systems.

Essential Developmental Function of Kinesin-II in Sea Urchin Embryos

The formation of normal motile cilia on sea urchin blastomeres is essential for embryonic motility and feeding (Masuda, 1979; Masuda and Sato, 1984; Stephens, 1995). Taken together, the data presented here provide strong evidence that the heterotrimeric kinesin-II motor protein plays a critical role in the assembly of motile 9+2 cilia on blastula-stage sea urchins and is thus essential for embryonic viability.

We would like to thank David Meyer for assistance in immunoblotting; Grete Fry, Robert Munn, and Paul Lee for expert technical advice and support on EM; William Dentler (University of Kansas, Lawrence, KS), Elizabeth Smith (University of Minnesota, Minneapolis, MN), and Samuel Bowser (Wadsworth Center, Albany, NY) for helpful discussions on cilia; and Shari Morris and the members of the Scholey lab for discussions and encouragement.

In addition, we gratefully acknowledge support from National Institutes of Health (NIH) grant GM50718 to J.M. Scholey and NIH postdoctoral fellowship GM17516 to R.L. Morris.

Received for publication 13 December 1996 and in revised form 18 July 1997.

References

Aizawa, H., Y. Sekine, R. Tekamura, Z. Zhang, M. Nangaku, and N. Hirokawa. 1992. Kinesin family in murine central nervous system. *J. Cell Biol.* 119: 1287–1296.

Auclair, W., and B.W. Siegel. 1966. Cilia regeneration in the sea urchin embryo: evidence for a pool of ciliary proteins. *Science (Wash. DC).* 154:913–915.

Beech, P.L., K. Pagh-Roehl, Y. Noda, N. Hirokawa, B. Burnside, and J.L. Rosenbaum. 1996. Localization of kinesin superfamily proteins to the connecting cilium of fish photoreceptors. *J. Cell Sci.* 109:889–897.

Bernstein, M., and J.L. Rosenbaum. 1994. Kinesin-like proteins in the flagella of *Chlamydomonas. Trends Cell Biol.* 4:236–240.

Bi, G.-Q., R.L. Morris, G. Liao, J.M. Alderton, J.M. Scholey, and R.A. Steinhardt. 1997. Kinesin- and myosin-driven steps of vesicle recruitment for calcium-regulated exocytosis. *J. Cell Biol.* 138:999–1008.

Bloom, G.S., and S. Endow. 1994. Kinesins. *Protein Profile.* 1:1059–1116.

Brokaw, C. 1994. Control of flagellar bending: a new agenda based on dynein diversity. *Cell Motil. Cytoskel.* 28:199–204.

Brokaw, C.J., and R. Kamiya. 1987. Bending patterns of *Chlamydomonas* flagella: IV. Mutants with defects in inner and outer arms indicate differences in dynein arm function. *Cell Motil. Cytoskel.* 8:68–75.

Burns, R.G. 1973. Kinetics of regeneration of sea urchin cilia. *J. Cell Sci.* 13:55–67.

Burns, R.G. 1979. Kinetics of regeneration of cilia. II. Regeneration of animalized cilia. *J. Cell Sci.* 37:205–215.

Buster, D., and J.M. Scholey. 1991. Purification and assay of kinesin from sea urchin eggs and early embryos. *J. Cell Sci.* 14 (Suppl.):109–115.

Cole, D.G., and J.R. Rosenbaum. 1996. A flagellar heterotrimeric kinesin; putative cargo revealed by analysis of ts mutants. *Mol. Biol. Cell.* B145:272.

Cole, D.G., and J.M. Scholey. 1995. Purification of kinesin-related protein complexes from eggs and embryos. *Biophys. J.* 68:158s–162s.

Cole. D.G., W.Z. Cande, R.J. Baskin, D.A. Skoufias, C.J. Hogan, and J.M. Scholey. 1992. Isolation of a sea urchin egg kinesin-related protein using peptide antibodies. *J. Cell Sci.* 101:291–301.

Cole, D.G., S.W. Chinn, K.P. Wedaman, K. Hall, T. Vuong, and J.M. Scholey. 1993. Novel heterotrimeric kinesin-related protein purified from sea urchin eggs. *Nature (Lond.).* 366:268–270.

Dentler, W.L. 1990. Linkages between microtubules and membranes in cilia and flagella. *In* Ciliary and Flagellar Membranes. R.A. Bloodgood, editor. Plenum Press, New York. 31–66.

Dutcher, S.K. 1995. Flagellar assembly in two hundred and fifty easy-to-follow steps. *Trends Genet.* 11:398–404.

Euteneuer, U., and J.R. McIntosh. 1981. Polarity of some motility related microtubules. *Proc. Natl. Acad. Sci. USA.* 78:372–376.

Gindhart, J.G., and L.S.B. Goldstein. 1996. Armadillo repeats in the SpKAP115 subunit of kinesin-II. *Trends Cell Biol.* 6:415–416.

Goldstein, L.S.B. 1993. With apologies to Scheherazade: tails of 1001 kinesin motors. *Annu. Rev. Genet.* 27:319–351.

Hamaguchi, M.S., and Y. Hiramoto. 1986. Analysis of the role of astral rays in pronuclear migration in sand dollar eggs by the Colcemid-UV method. *Dev. Growth Diff.* 28:143–156.

Henson, J.H., D.G. Cole, M. Terasaki, D.J. Rashid, and J.M. Scholey. 1995. Immunolocalization of the heterotrimeric kinesin-related protein, KRP85/95 in the mitotic apparatus of sea urchin embryos. *Dev. Biol.* 171:182–194.

Henson, J.H., D.G. Cole, C.D. Roesener, S. Capuano, R.J. Mendola, and J.M. Scholey. 1997. The heterotrimeric motor protein, kinesin-II localizes to the midpiece and flagellum of sea urchin and sand dollar sperm. *Cell Motil. Cytoskel.* In press.

Ingold, A.L., S.A. Cohn, and J.M. Scholey. 1988. Inhibition of kinesin-driven microtubule motility by monoclonal antibodies to kinesin heavy chains. *J. Cell Biol.* 107:2657–2667.

Jensen, C.G., E.A. Davison, S.S. Bowser, and C.L. Rieder. 1987. Primary cilia in PtK_1 cells: effects of colcemid and taxol on cilia formation and resorption. *Cell Motil. Cytoskel.* 7:187–197.

Johnson, K.A., and J.L. Rosenbaum. 1992. Polarity of flagellar assembly in *Chlamydomonas. J. Cell Biol.* 119:1605–1611.

Kiehart, D.P. 1982. Microinjection of echinoderm eggs: apparatus and procedures. *Methods Cell Biol.* 25:13–31.

Kondo, S., R. Seiko-Yoshitake, Y. Noda, H. Aizawa, T. Nakata, Y. Matsuura, and N. Hirokawa. 1994. Kif3a is a new microtubule-based anterograde motor in the nerve axon. *J. Cell Biol.* 125:1095–1107.

Kozminski, K.G., K.A. Johnson, P. Forscher, and J.L. Rosenbaum. 1993. A motility in the eukaryotic flagellum unrelated to flagellar beating. *Proc. Natl. Acad. Sci. USA.* 90:5519–5523.

Kozminski, K.G., P.L. Beech, and J.L. Rosenbaum. 1995. The *Chlamydomonas* kinesin-like protein FLA10 is involved in motility associated with the flagellar membrane. *J. Cell Biol.* 131:1517–1527.

Lepage, T., C. Sardet, and C. Gache. 1992. Spatial expression of the hatching enzyme gene in the sea urchin embryo. *Dev. Biol.* 150:23–32.

Linck, R.W., and G.L. Langevin. 1982. Structure and chemical composition of insoluble filamentous components of sperm flagellar microtubules. *J. Cell Sci.* 58:1–22.

Lux, F.G., III, and S.K. Dutcher. 1991. Genetic interactions at the FLA10 Locus: suppressors and synthetic phenotypes that affect the cell cycle and flagellar function in *Chlamydomonas reinhardtii. Genetics.* 128:549–561.

Masuda, M. 1979. Species specific pattern of ciliogenesis in developing sea urchin embryos. *Dev. Growth Diff.* 21:545–552.

Masuda, M., and H. Sato. 1984. Reversible resorption of cilia and the centriole cycle in dividing cells of sea urchin blastulae. *Zool. Sci.* 1:445–462.

Menco, B. 1980. Qualitative and quantitative freeze-fracture studies on olfactory and nasal respiratory structures of frog, ox, rat, and dog. I. A general survey. *Cell Tiss. Res.* 207:183–209.

Miller, J.M., W. Wang, R. Balczon, and W.L. Dentler. 1990. Ciliary microtubules contain a mammalian kinetochore antigen. *J. Cell Biol.* 110:703–714.

Minamide, L.S., and J.R. Bamburg. 1990. A filter-paper dye-binding assay for quantitative determination of protein without interference from reducing agents or detergents. *Anal. Biochem.* 190:66–70.

Norrander, J.M., R.W. Linck, and R.E. Stephens. 1995. Transcriptional control of tektin A mRNA correlates with cilia development and length determination during sea urchin embryogenesis. *Development (Camb.).* 121:1615–1623.

Pesavento, P.A., R.J. Stewart, and L.S.B. Goldstein. 1994. Characterization of the KLP68D kinesin-like protein in *Drosophila*: possible roles in axonal transport. *J. Cell Biol.* 127:1041–1048.

Piperno, G., and K. Mead. 1997. Transport of a novel complex in the cytoplasmic matrix of *Chlamydomonas* flagella. *Proc. Natl. Acad. Sci. USA*. 94:4457–4462.

Piperno, G., and Z. Ramanis. 1991. The proximal portion of *Chlamydomonas* flagella contains a distinct set of inner dynein arms. *J. Cell Biol.* 112:701–709.

Piperno, G., K. Mead, and S. Henderson. 1996. Inner dynein arms but not outer dynein arms require the activity of kinesin homologue protein KHP1-FLA10 to reach the distal part of flagella in *Chlamydomonas. J. Cell Biol.* 133:371–379.

Poole, A.C., M.H. Flint, and B.W. Beaumont. 1985. Analysis of the morphology and function of primary cilia in connective tissues: a cellular cybergenetic probe? *Cell Motil.* 5:175–193.

Pryer, N.K., P. Wadsworth, and E.D. Salmon. 1986. Polarized microtubule gliding and particle saltations produced by soluble factors from sea urchin eggs and embryos. *Cell Motil. Cytoskel.* 6:537–548.

Rappaport, R. 1996. Cytokinesis in Animal Cells. Cambridge University Press, Cambridge, UK. 386 pp.

Rashid, D.J., K.P. Wedaman, and J.M. Scholey. 1995. Heterodimerization of the two motor subunits of the heterotrimeric kinesin, KRP(85/95). *J. Mol. Biol.* 252:157–162.

Rogers, S.L., I.S. Tint, P.C. Fanapour, and V.I. Gelfand. 1997. Regulated bidirectional motility of melanophore pigment granules along microtubules *in vitro. Proc. Natl. Acad. Sci. USA*. 94:3720–3725.

Roth, K.E., E.A. Davison, N. Myers, C.L. Rieder, and S.S. Bowser. 1987. Correlative light and electron microscopy of primary (9+0) cilia in cultured kidney epithelial cells. *In* Proceedings of the 45th Annual Meeting of the Electron Microscopy Society of America. G.W. Bailey, editor. San Francisco Press, Inc., San Francisco, CA. 828–829.

Roth, K.E., C.L. Rieder, and S.S. Bowser. 1988. Flexible substratum technique for viewing cells from the side: some in vivo properties of primary (9+0) cilia in cultured kidney epithelia. *J. Cell Sci.* 89:457–466.

Scholey, J.M. 1996. Kinesin-II, a membrane traffic motor in axons, axonemes, and spindles. *J. Cell Biol.* 133:1–4.

Scholey, J.M., M.E. Porter, P.M. Grissom, and J.R. McIntosh. 1985. Identification of kinesin in sea urchin eggs and evidence for its localization in the mitotic spindle. *Nature (Lond.)*. 318:483–486.

Scholey, J.M., J. Heuser, J.T. Yang, and L.S.B. Goldstein. 1989. Identification of globular mechanochemical heads of kinesin. *Nature (Lond.)*. 338:355–357.

Schroeder, T.E. 1987. Fourth cleavage of sea urchin blastomeres: microtubule patterns and myosin localization in equal and unequal cell divisions. *Dev. Biol.* 124:9–22.

Skoufias, D.A., D.G. Cole, K.P. Wedaman, and J.M. Scholey. 1994. The carboxyl-terminal domain of kinesin heavy chain is important for membrane binding. *J. Biol. Chem.* 269:1477–1485.

Smith, E.F., and P. Lefebvre. 1996. PF16 encodes a protein with armadillo repeats that localizes to a single microtubule of the central apparatus in *Chlamydomonas* flagella. *J. Cell Biol.* 132:359–370.

Sorokin, S.P. 1968. Reconstruction of centriole formation and ciliogenesis in mammalian lungs. *J. Cell Sci.* 3:207–230.

Steinhardt, R.A., G. Bi, and J.M. Alderton. 1994. Cell membrane resealing by a vesicular mechanism similar to neurotransmitter release. *Science (Wash. DC)*. 263:390–393.

Stephens, R.E. 1986. Isolation of embryonic cilia and sperm flagella. *Methods Cell Biol.* 27:217–227.

Stephens, R.E. 1989. Quantal tektin synthesis and ciliary length in sea urchin embryos. *J. Cell Sci.* 92:403–413.

Stephens, R.E. 1995. Ciliogenesis in sea urchin embryos—a subroutine in the program of development. *BioEssays.* 17:331–340.

Tabish, M., Z.K. Siddiqui, K. Nishikawa, and S.S. Siddiqui. 1995. Exclusive expression of *C. elegans* Osm-3 kinesin gene in chemosensory neurons open to the external environment. *J. Mol. Biol.* 247:377–389.

Terasaki, M., and L.A. Jaffe. 1991. Organization of the sea urchin egg endoplasmic reticulum and its reorganization at fertilization. *J. Cell Biol.* 114:929–940.

Vale, R.D., and R. Fletterick. 1997. The design plan of kinesin motors. *Annu. Rev. Cell Dev. Biol.* In press.

Vashishtha, M., Z. Walther, and J.L. Hall. 1996. The kinesin-homologous protein encoded by the *Chlamydomonas* FLA10 gene is associated with basal bodies and centrioles. *J. Cell Sci.* 109:541–549.

Wadsworth, P. 1987. Microinjected carboxylated beads move predominantly poleward in sea urchin eggs. *Cell Motil. Cytoskel.* 8:293–301.

Walther, Z., M. Vashishtha, and J.L. Hall. 1994. The *Chlamydomonas* FLA10 gene encodes a novel kinesin-homologous protein. *J. Cell Biol.* 126:175–188.

Wedaman, K.P., D.W. Meyer, D.J. Rashid, D.G. Cole, and J.M. Scholey. 1996. Sequence and submolecular localization of the 115-kD accessory subunit of the heterotrimeric kinesin-II (KRP85/95) complex. *J. Cell Biol.* 132:371–380.

Wheatley, D.N. 1995. Primary cilia in normal and pathological tissues. *Pathobiology.* 63:222–238.

Wheatley, D.N., A.M. Wang, and G.E. Strugnell. 1996. Expression of primary cilia in mammalian cells. *Cell Biol. Int.* 20:73–81.

Wright, B.D., and J.M. Scholey. 1992. Microtubule motors in the early sea urchin embryo. *Curr. Top. Dev. Biol.* 26:71–91.

Wright, B.D., J.H. Henson, K.P. Wedaman, P.J. Willy, J.N. Morand, and J.M. Scholey. 1991. Subcellular localization and sequence of sea urchin kinesin heavy chain—evidence for its association with membranes in the mitotic apparatus and interphase cytoplasm. *J. Cell Biol.* 113:817–833.

Wright, B.D., M. Terasaki, and J.M. Scholey. 1993. Roles of kinesin and kinesin-like proteins in sea urchin embryonic cell division: evaluation using antibody microinjection. *J. Cell Biol.* 123:681–689.

Yamazaki, H., T. Nakata, Y. Okada, and N. Hirokawa. 1995. Kif3a/3b: a heterodimeric kinesin superfamily protein that works as a microtubule plus end–directed motor for membrane organelle transport. *J. Cell Biol.* 130: 1387–1399.

Zar, J.H. 1984. Biostatistical Analysis. 2nd Ed. Prentice Hall, Inc., Englewood Cliffs, NJ. 718 pp.